Supplement of Clim. Past, 22, 1537–1557, 2026
https://doi.org/10.5194/cp-22-1537-2026-supplement

Climate of the Past
Open Access

Supplement of

Holocene hydroclimatic variability and multi-frequency analyses at Lake Sidi Ali (Morocco)

Johannes Schmidt et al.

Correspondence to: Johannes Schmidt (j.schmidt@uni-leipzig.de)

Abstract

The Supplementary Material provides additional methodological details, figures and statistical analyses supporting the interpretation of Holocene hydroclimatic variability at Lake Sidi Ali. It includes the complete Redfit analyses of the original XRF-derived proxy data, grouped according to the Redfit Proxy Groups (RPGs), as well as the corresponding wavelet analyses of all investigated XRF proxies. In addition, principal component analyses (PCA) were conducted on both the extracted spectral properties of the proxies (PCA_{freq}) and the original XRF-derived proxy data in the time domain (PCA_{time}). The PCA_{freq} analysis serves as an additional statistical approach to evaluate the grouping of proxies in the frequency domain, whereas the PCA_{time} analysis assesses the dominant variability structures within the original proxy dataset. Furthermore, the Supplementary Material contains additional figures and methodological information complementing the analyses presented in the main manuscript. Overall, the Supplementary Material aims to strengthen the methodological transparency and robustness of the study and to provide additional clarity regarding the statistical and palaeoenvironmental interpretations discussed in the main text.

S1 Redfit analyses of original XRF-based proxy data

The following figures show the complete Redfit periodograms of all analysed XRF-derived proxies grouped according to the RPG classification presented in the main manuscript.

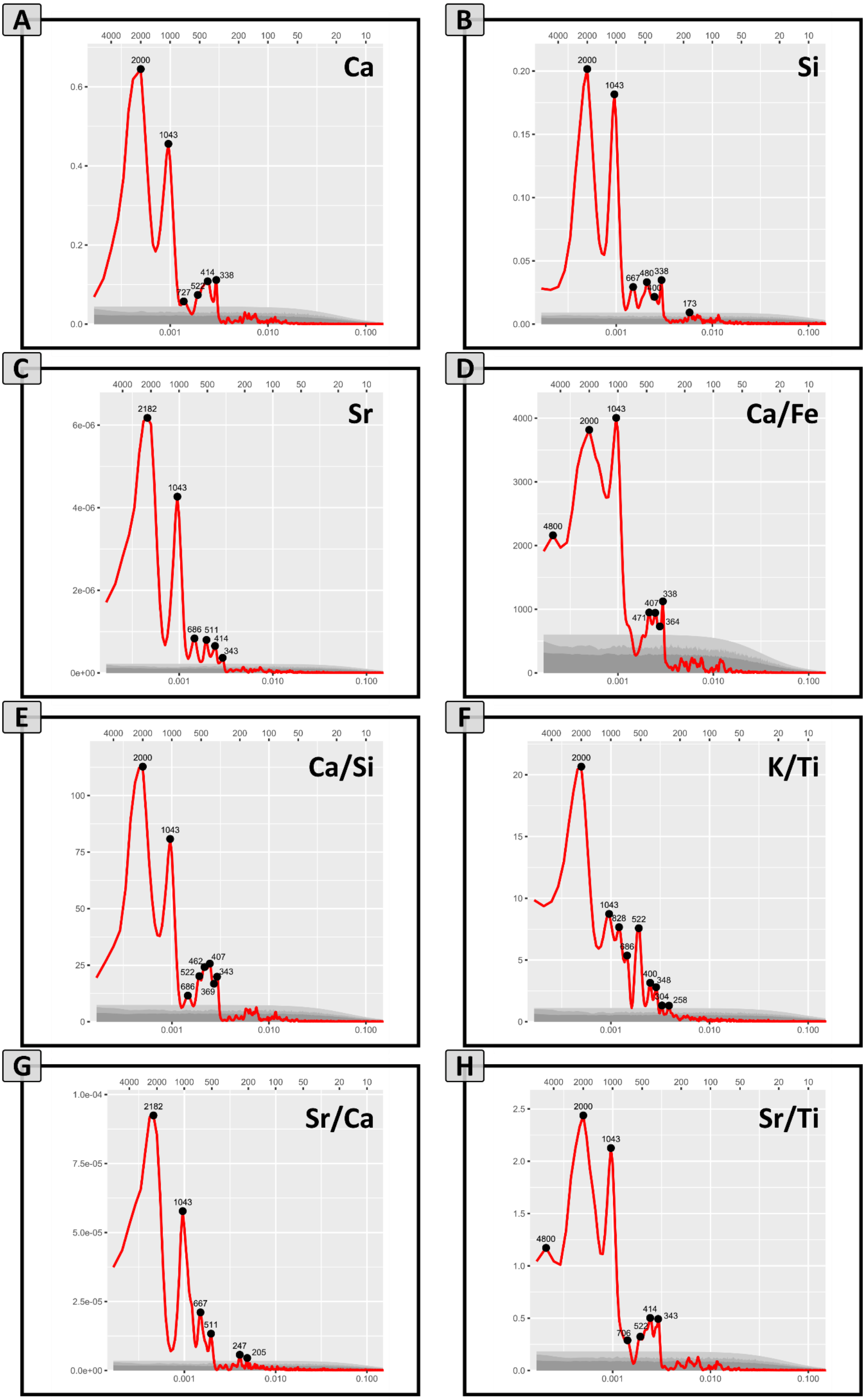

A
Ca
B
Si
C
Sr
D
Ca/Fe
E
Ca/Si
F
K/Ti
G
Sr/Ca
H
Sr/Ti

Figure S1: Redfit power spectra of XRF-scan-based proxies from Redfit Proxy Group 1; A) Calcium, B) Silicon, C) Strontium, D) Calcium/Iron ratio, E) Calcium/Silicon ratio, F) Potassium/Titanium ratio, G) Strontium/Calcium ratio, H) Strontium/Titanium ratio. Each Y-axis represents the power value of respective proxy. Each x-axis represents the frequency (lower label) and period in years (upper label). Grey areas show the significance level (darkest grey – 95%, dark grey – 99%, light grey – crit. Level). Black dots with numbers show local peaks with periodicity in years that are significant at the highest crit. Level.

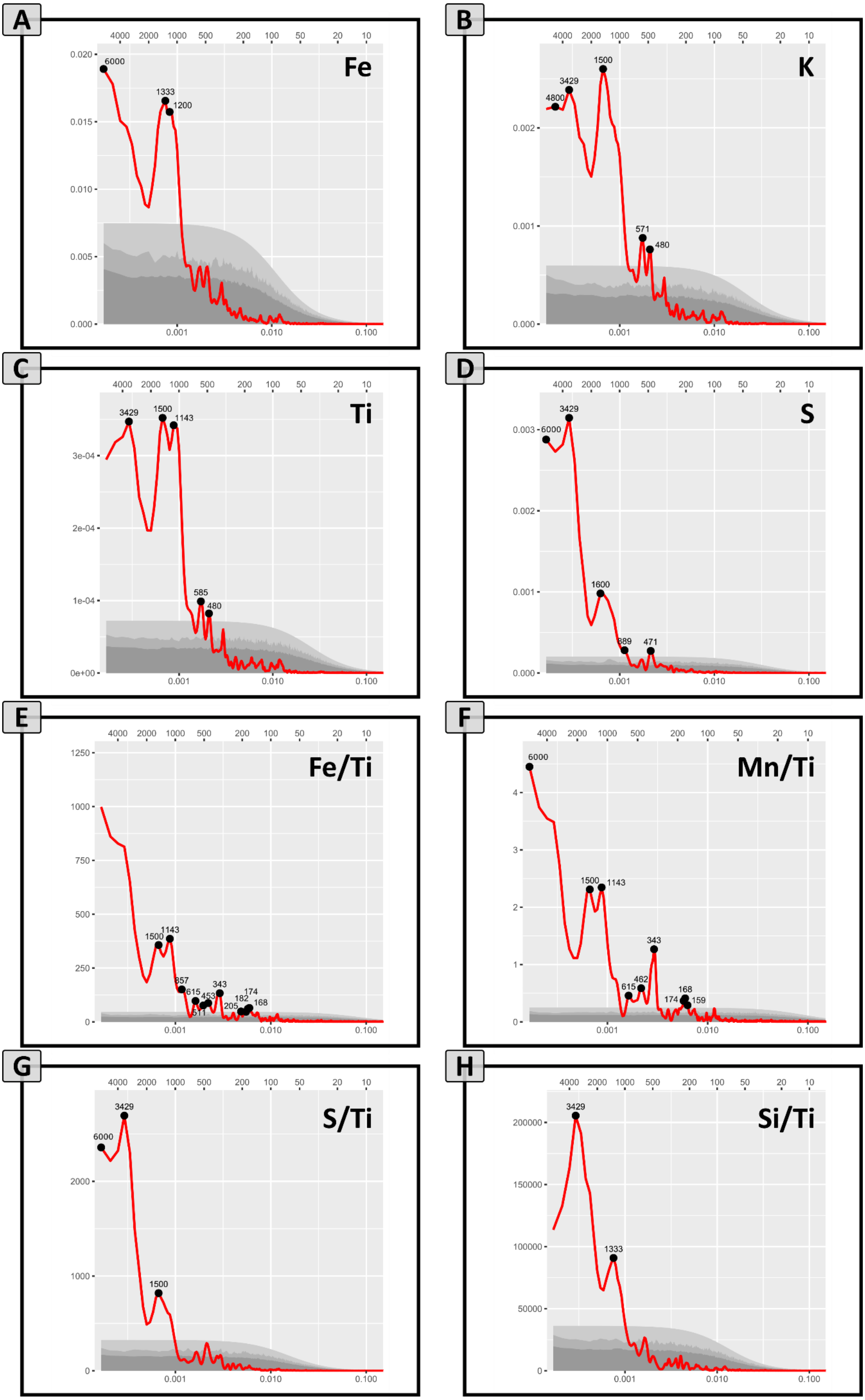
A
Fe
6000
1333
1200
B
K
4800
3429
1500
571
480
C
Ti
3429
1500
1143
585
480
D
S
6000
3429
1600
389
471
E
Fe/Ti
1500
1143
857
615
453
511
343
182
205
174
168
F
Mn/Ti
6000
1500
1143
343
462
615
168
174
159
G
S/Ti
6000
3429
1500
H
Si/Ti
3429
1333
4000 2000 1000 500 200 100 50 20 10
0.001
0.010
0.100

Figure S2: Redfit power spectra of XRF-scan-based proxies from Redfit Proxy Group 2; A) Iron, B) Potassium, C) Titanium, D) Sulfur, E) Iron/Titanium ratio, F) Manganese/Titanium ratio, G) Sulfur/Titanium ratio, H) Silicon/Titanium ratio. Each Y-axis represents the power value of respective proxy. Each x-axis represents the frequency (lower label) and period in years (upper label). Grey areas show the significance level (darkest grey – 95%, dark grey – 99%, light grey – crit. Level). Black dots with numbers show local peaks with periodicity in years that are significant at the highest crit. Level.

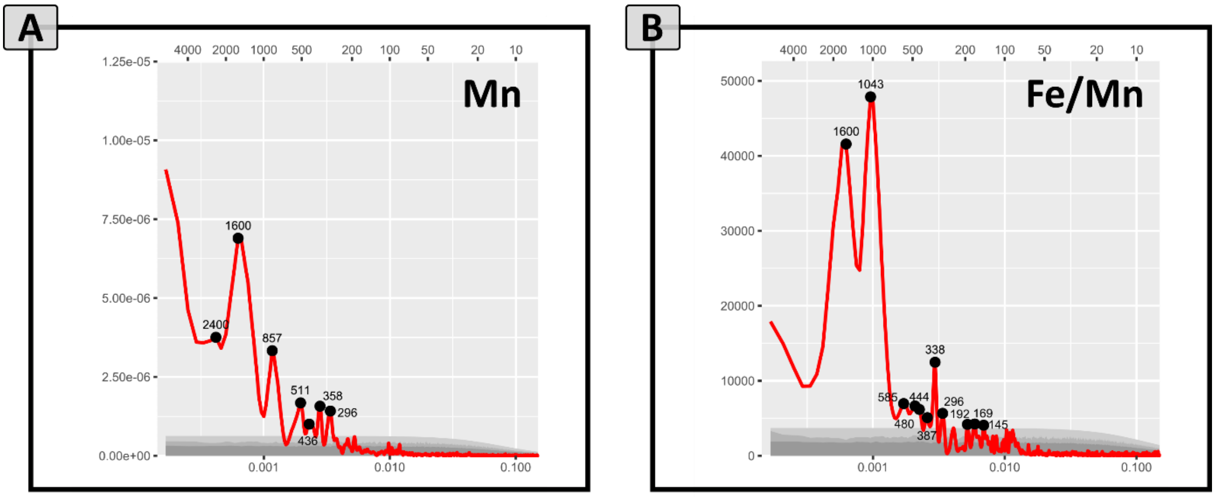

Figure S3: Redfit power spectra of XRF-scan-based proxies from Redfit Proxy Group 3; A) Manganese, B) Iron/Manganese ratio. Each Y-axis represents the power value of respective proxy. Each x-axis represents the frequency (lower label) and period in years (upper label). Grey areas show the significance level (darkest grey – 95%, dark grey – 99%, light grey – crit. Level). Black dots with numbers show local peaks with periodicity in years that are significant at the highest crit. Level.

S2 Wavelet analyses of original XRF-based proxy data

The following figures show the complete Wavelet power spectra of all analysed XRF-derived proxies grouped according to the RPG classification presented in the main manuscript.

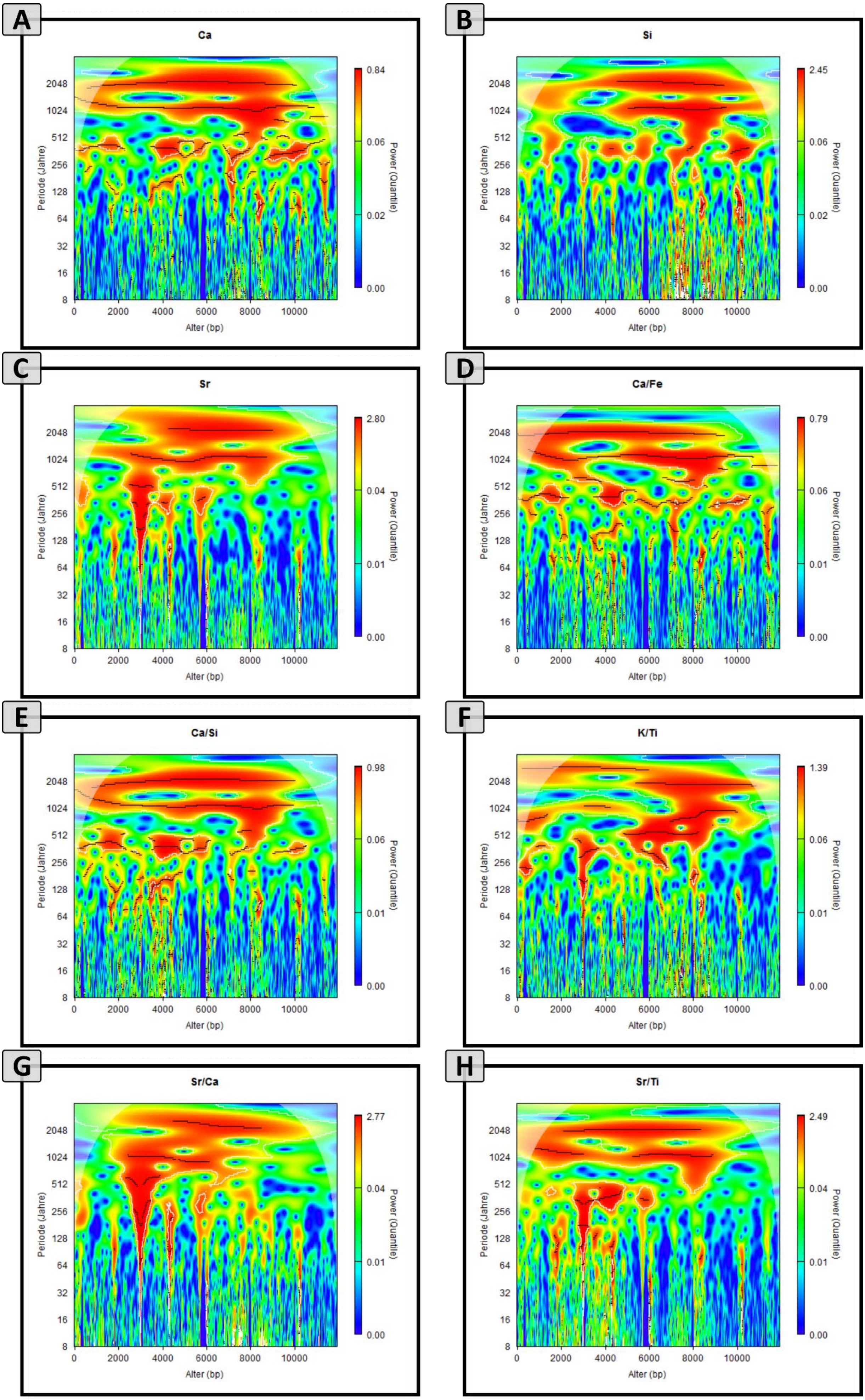

A
Ca
B
Si
C
Sr
D
Ca/Fe
E
Ca/Si
F
K/Ti
G
Sr/Ca
H
Sr/Ti
Periode (Jahre)
Alter (bp)
Power (Quantile)

Figure S4: Wavelet power spectra of XRF-scan-based proxies from Redfit Proxy Group 1; A) Calcium, B) Silicon, C) Strontium, D) Calcium/Iron ratio, E) Calcium/Silicon ratio, F) Potassium/Titanium ratio, G) Strontium/Calcium ratio, H) Strontium/Titanium ratio. Colours show the specific power values. White lines enclose the significant areas and black lines local maxima. Grey facet shows the cone of influence.

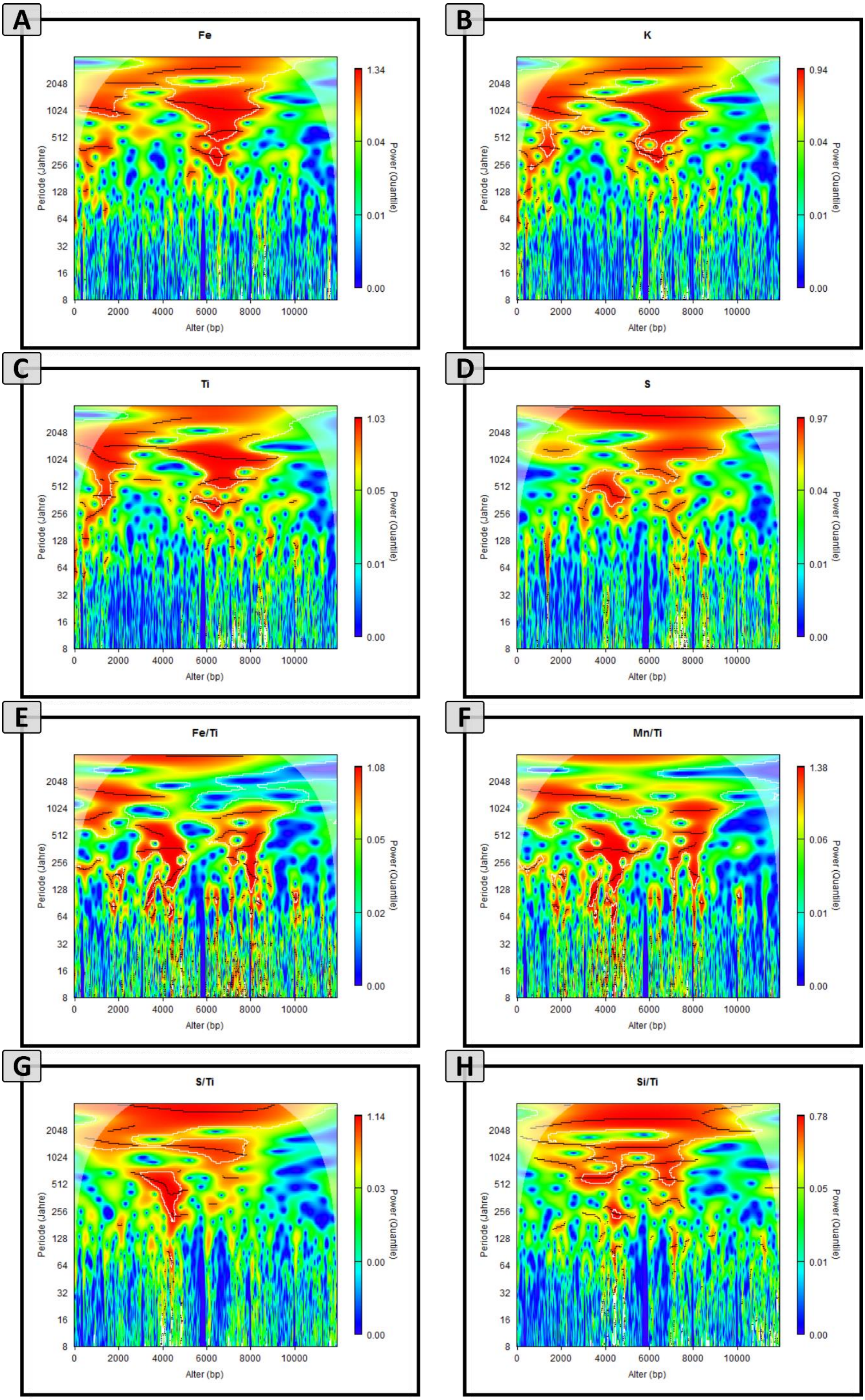
A
Fe
1.34
0.04
0.01
0.00
B
K
0.94
0.04
0.01
0.00
C
Ti
1.03
0.05
0.01
0.00
D
S
0.97
0.04
0.01
0.00
E
Fe/Ti
1.08
0.05
0.02
0.00
F
Mn/Ti
1.38
0.06
0.01
0.00
G
S/Ti
1.14
0.03
0.00
0.00
H
Si/Ti
0.78
0.05
0.01
0.00
Periode (Jahre)
2048
1024
512
256
128
64
32
16
8
Alter (bp)
0
2000
4000
6000
8000
10000
Power (Quantile)

Figure S5: Wavelet power spectra of XRF-scan-based proxies from Redfit Proxy Group 2; A) Iron, B) Potassium, C) Titanium, D) Sulfur, E) Iron/Titanium ratio, F) Manganese/Titanium ratio, G) Sulfur/Titanium ratio, H) Silicon/Titanium ratio. Colours show the specific power values. White lines enclose the significant areas and black lines local maxima. Grey facet shows the cone of influence.

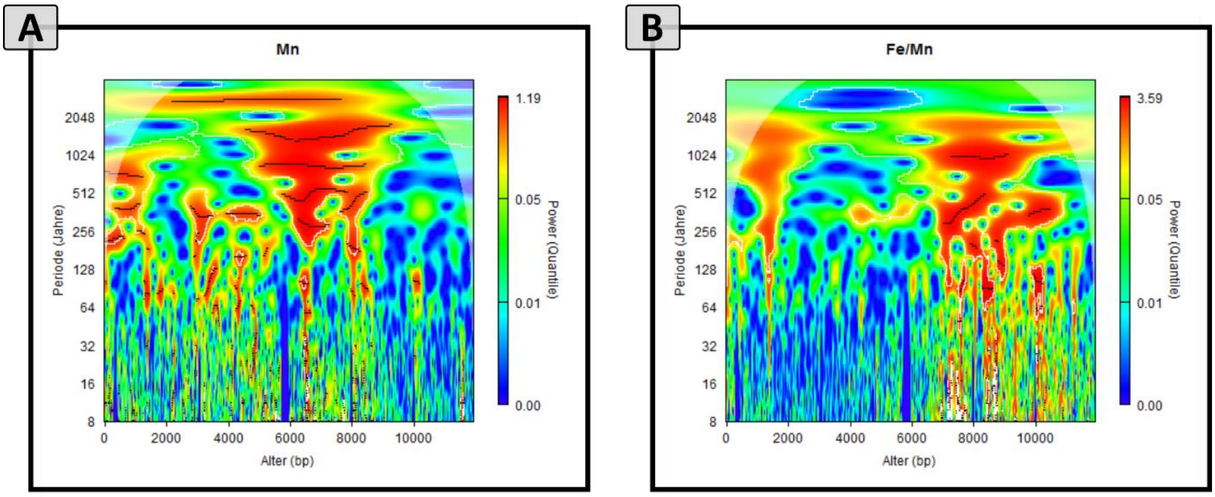

Figure S6: Wavelet power spectra of XRF-scan-based proxies from Redfit Proxy Group 3; A) Manganese, B) Iron/Manganese ratio. Colours show the specific power values. White lines enclose the significant areas and black lines local maxima. Grey facet shows the cone of influence.

S3 PCA analyses

S3.1 XRF-based proxy data in frequency domain (PCA_{freq}) To further evaluate the robustness of the frequency-domain proxy grouping, a principal component analysis (PCA_{freq}) was conducted using the extracted significant spectral information from the Redfit analyses as input data. The PCA_{freq} approach provides an additional multivariate assessment of similarities among the spectral properties of the investigated proxies and complements the correlation-based grouping procedure presented in the main manuscript. Furthermore, the PCA_{freq} results (**Figure S7**) reveal grouping patterns comparable to those derived from the correlation analysis (**Fig. 2D** in main text) of the significant Redfit spectra. For the PCA calculations, we used the function *prcomp()* from the stats package within the R (R Core Team, 2020).

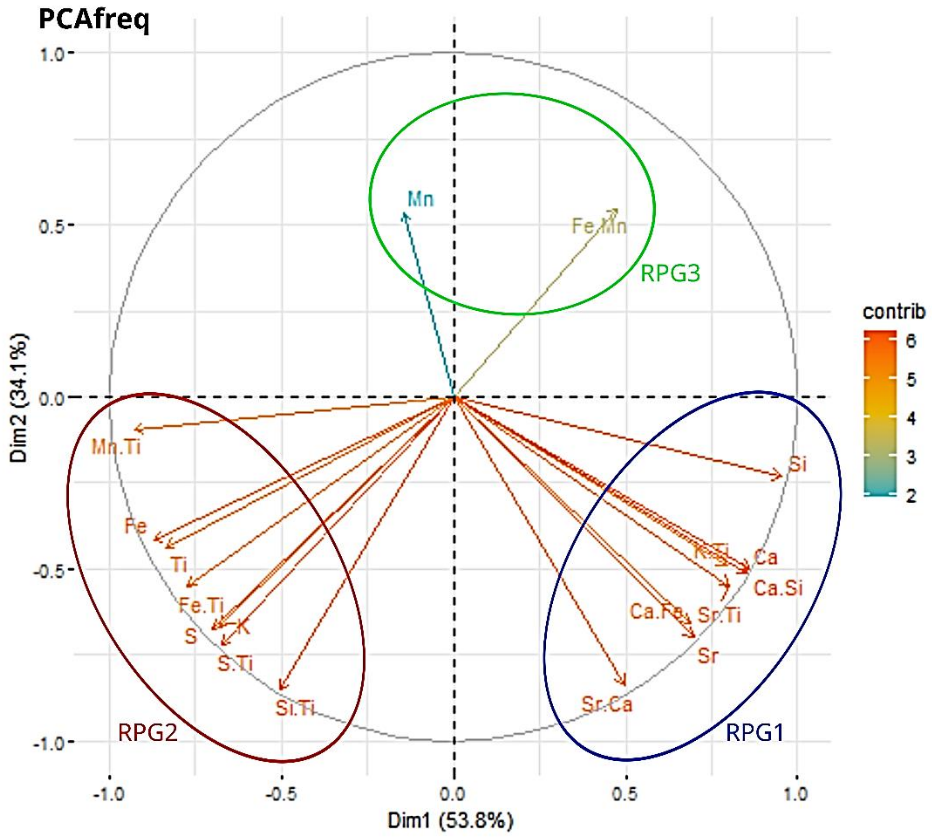

Figure S7: PCA biplot of the first two principal components (PC1 and PC2, that explain 87.9 % of the variance) derived from the spectral properties of the XRF-based proxies (PCA_{freq}). Dots in the proxy denomination represents ratios (e.g. Fe.Mn in the figure is Fe/Mn). Arrows represent the loadings of the individual proxies and illustrate their contribution and direction within the multivariate parameter space. Warm colours represent variables with a stronger influence on the orientation of the principal component space, whereas cool colours indicate lower contributions. Proxies showing similar orientations and clustering patterns indicate comparable variability structures within the frequency domain. Three major groups (RPGs) of input variables are visible.

S3.2 XRF-based proxy data in time domain (PCA_{time})

In addition to the frequency-domain PCA, a second principal component analysis (PCA_{time}) was performed using the original XRF-derived proxy time series as input data. The aim of this analysis is to evaluate the dominant variability structures within the original proxy dataset independent of the Redfit-based grouping approach.

The results of the PCA_{time} analysis (**Figure S8**), particularly the loading patterns, reveal a grouping of the XRF proxies that differs from the proxy classification derived from the spectral analyses (**Fig. 2D** in the main text and **Figure S7**). PC1 (Dim. 1; 56.5 % explained variance)) is dominated by XRF proxies belonging to both RPG 1 and RPG 2. However, no clear opposition ("seesaw") between these two groups is apparent. Instead, proxies from both RPG 1 and RPG 2 show positive as well as negative correlations with PC1. In contrast, PC2 (Dim. 2; 26.5 % explained variance) is positively correlated with S, S/Ti and Si/Ti. PC3 (Dim. 3; 11.2 % explained variance) does not reveal a clear structure in relation to the identified RPGs. Overall, the grouping structure that emerges from the PCA_{time} analysis differs from the RPG classification derived from the spectral analyses, indicating that the dominant covariance structures in the time domain are not identical to the coherence patterns observed in the frequency domain.

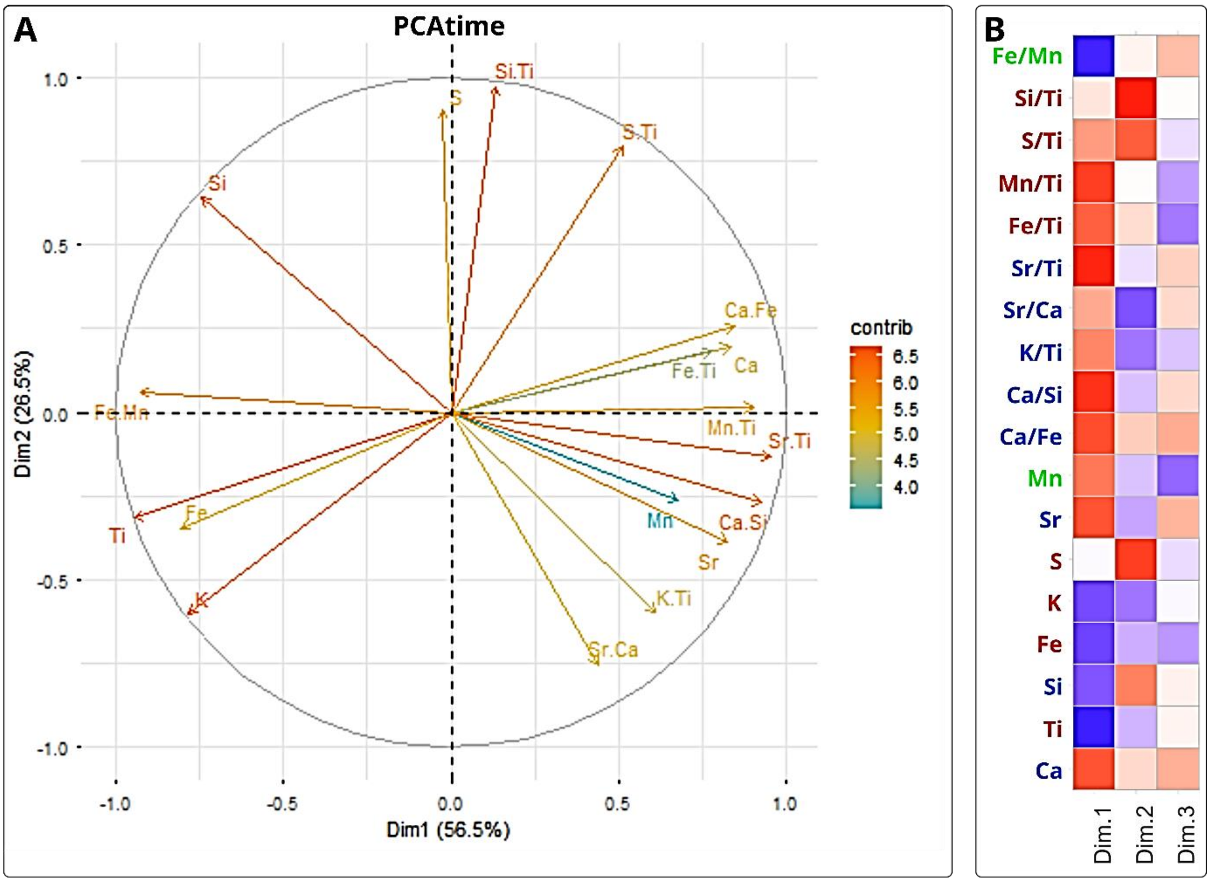

Figure S8: A) PCA biplot of the first two principal components (PC1 and PC2, that explain 83 % of the variance) derived from the original XRF-based proxy time series (PCA_{time}). Dots in the proxy denomination represents ratios (e.g. Fe.Mn in the figure is Fe/Mn). Arrows represent the loadings of the individual proxies and illustrate their contribution and direction within the multivariate parameter space. Warm colours represent variables with a stronger influence on the orientation of the principal component space, whereas cool colours indicate lower contributions. Proxies showing similar orientations and clustering patterns indicate comparable variability structures within the time domain. B) Correlation plot (method = "Spearman") of the PCA_{time} loadings for the first three principal components. Proxy labels are colour-coded according to the Redfit Proxy Groups (RPGs) identified in the main manuscript, with RPG 1 shown in blue, RPG 2 in red and RPG 3 in green.

S4 Spectral Analyses of PCA_{time} scores

The first three principal component scores were processed using the same (pre-) processing workflow (see Material and Methods section in main manuscript) as the original proxy data, including detrending, Redfit and Wavelet analyses. This allows a direct comparison between the spectral properties of the principal components and those derived from the original proxy records.

Based on the Redfit analyses of the first three principal components (**Figure S9 A-C**) derived from the PCA_{time} analysis, the following robust periodicities can be identified:

PC1 – robust cycles: 6000 y, 2000 y, 1043 y, 545 y, 471 y, 338 y

PC2 – robust cycles: 3429 y, 1600 y

PC3 – robust cycles: 2667 y, 1091 y, 727 y, 490 y, 403 y, 348 y, 304 y

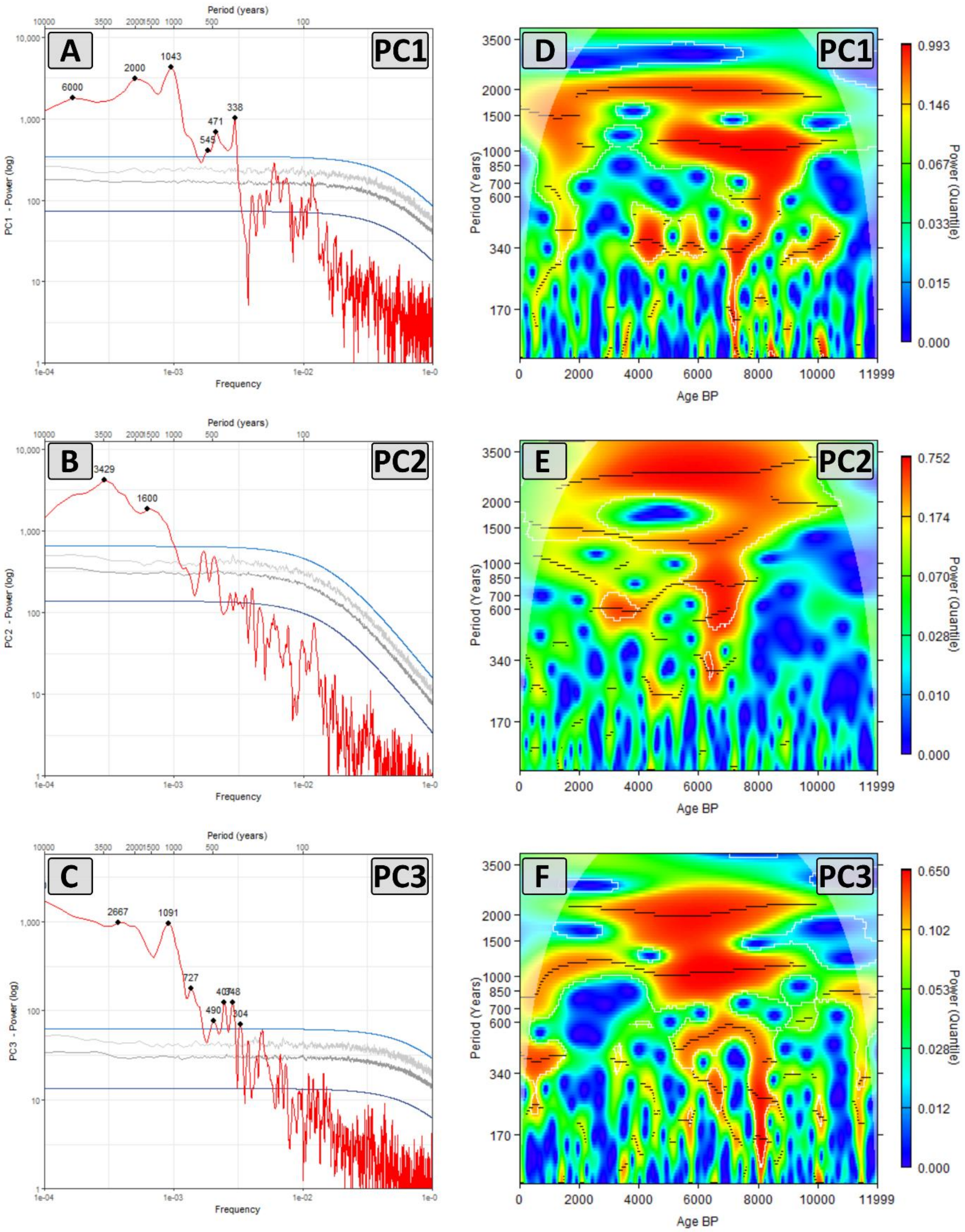

Figure S9: Redfit periodograms (A–C) and wavelet power spectra (D–F) of the first three principal components (PC1–PC3) derived from the PCA_{time} analysis of the original XRF-based proxy dataset. (A) Redfit periodogram of PC1, (B) Redfit periodogram of PC2 and (C) Redfit periodogram of PC3. In panels A–C, the y-axis represents the spectral power values of the respective principal component, whereas the x-axis shows the frequency (lower axis) and the corresponding period in years (upper axis). Black dots and labels indicate local spectral peaks with periodicities that are significant at the highest critical significance level. Panels (D–F) show the corresponding wavelet power spectra for PC1–PC3. Colours indicate the magnitude of the wavelet power values. White contours enclose statistically significant areas, black lines mark local maxima, and the grey-shaded regions represent the cone of influence, where edge effects reduce the reliability of the spectral information.

S5 Discussion of differences between RPGs and PCA_{time} grouping results

Although the robust periodicities identified from the Redfit and wavelet analyses of the first principal components of the PCA_{time} analysis are broadly comparable to those observed in the original proxy-based spectral analyses, the grouping of the elemental proxies differs between both approaches. In the original workflow, the Redfit Proxy Groups (RPGs) were derived directly from the spectral characteristics of the individual proxy records, whereas the PCA_{time} approach first transforms the original proxy dataset into orthogonal principal components prior to the spectral analyses.

A principal component analysis (PCA) combines the input variables linearly within the component scores. This can modify the original spectral signal and may strengthen, weaken, or artificially introduce periodicities (Gallant et al., 2018). Therefore, we aimed to conduct the time-series statistics, as far as possible, using the original ("raw") proxy data rather than transformed component scores. For this reason, the proxy grouping was primarily carried out on the basis of their spectral characteristics. It was important for us to retain the analyses as long as possible within the original/raw-data domain and to calculate the spectral properties directly from these proxy records. A PCA can be a useful approach for reducing the dimensionality of XRF elemental datasets (Bertrand et al., 2024; Evans et al., 2019). The use of PCA scores from the dominant principal components for spectral analyses has occasionally been applied in recent studies (Ferreira et al., 2025; Gebregiorgis et al., 2020). However, this procedure mixes the original proxy signals and may alter their spectral characteristics. For example, phase shifts in the original proxy data may lead to distortions in the resulting principal components. We therefore argue that the difference in proxy distributions between the RPG classification and the PCA_{time} grouping are likely related to the linear mixing of the proxy signals during PCA ordination, whereas the original RPG approach preserves the individual spectral behaviour of the proxy records more directly.

S6 Tables

Table S1: *Compilation of used XRF proxies related to the XRF proxy compilations (Cohen, 2003; Davies et al., 2015) . Appropriate to available elements, including extracted "standard" climatic signals and process signal.*

No.	Proxy	Climate signal	Process signal	Reference
1	Ca	Precipitation, Temperature	Evaporation, Bioproductivity, Erosion	Davies et al. 2015, Cohen 2003
2	Ca/Fe	other	Erosion	Davies et al. 2015
3	Ca/Si	Temperature	Other	Davies et al. 2015
4	Fe	Precipitation	Evaporation, Erosion, Redox	Davies et al. 2015, Cohen 2003
5	Fe/Mn	Precipitation	Redox	Davies et al. 2015, Cohen 2003
6	Fe/Ti	Precipitation	Evaporation, Erosion, Redox	Davies et al. 2015
7	K	Precipitation	Erosion	Davies et al. 2015, Cohen 2003
8	K/Ti	Precipitation, Temperature	Other	Davies et al. 2015
9	Mn	Precipitation	Evaporation, Erosion, Redox	Davies et al. 2015, Cohen 2003
10	Mn/Ti	Precipitation, Temperature	Redox	Davies et al. 2015
11	S	Temperature	Evaporation, Bioproductivity	Davies et al. 2015, Cohen 2003
12	S/Ti	Other	Evaporation, Bioproductivity	Davies et al. 2015
13	Si	Precipitation, Temperature	Erosion, Bioproductivity	Davies et al. 2015, Cohen 2003
14	Si/Ti	Temperature	Bioproductivity	Davies et al. 2015
15	Sr	Other	Evaporation, Bioproductivity, Erosion	Davies et al. 2015, Cohen 2003
16	Sr/Ca	Temperature	Bioproductivity	Davies et al. 2015, Cohen 2003
17	Sr/Ti	Temperature	Bioproductivity	Davies et al. 2015
18	Ti	Precipitation	Erosion	Davies et al. 2015, Cohen 2003

References

Bertrand, S., Tjallingii, R., Kylander, M. E., Wilhelm, B., Roberts, S. J., Arnaud, F., Brown, E., and Bindler, R.: Inorganic geochemistry of lake sediments: A review of analytical techniques and guidelines for data interpretation, Earth-Science Reviews, 249, 104639, https://doi.org/10.1016/j.earscirev.2023.104639, 2024.

Cohen, A. S.: Paleolimnology: The history and evolution of lake systems, New York; Oxford University Press, Oxford, 500 pp., 2003.

Davies, S. J., Lamb, H. F., and Roberts, S. J.: Micro-XRF Core Scanning in Palaeolimnology: Recent Developments, in: Micro-XRF Studies of Sediment Cores, edited by: Croudace, I. W. and Rothwell, R. G., Springer Netherlands, Dordrecht, 189–226, https://doi.org/10.1007/978-94-017-9849-5_7, 2015.

Evans, G., Augustinus, P., Gadd, P., Zawadzki, A., and Ditchfield, A.: A multi-proxy µ-XRF inferred lake sediment record of environmental change spanning the last ca. 2230 years from Lake Kanono, Northland, New Zealand, Quaternary Science Reviews, 225, 106000, https://doi.org/10.1016/j.quascirev.2019.106000, 2019.

Ferreira, P. A. de L., de Mahiques, M. M., Sartoretto, J. R., and Figueira, R. C. L.: Evidence of anthropogenic and climate-related processes derived from metal contents in sediment cores from a heavily industrialized subtropical estuary, Environ Earth Sci, 84, 154, https://doi.org/10.1007/s12665-025-12168-6, 2025.

Gallant, D., Gallo, L. C., and Parker, M. L.: X-ray spectral variability of blazars using principal component analysis, Mon Not R Astron Soc, 480, 1999–2010, https://doi.org/10.1093/mnras/sty1987, 2018.

Gebregiorgis, D., Giosan, L., Hathorne, E. C., Anand, P., Nilsson-Kerr, K., Plass, A., Lückge, A., Clemens, S. C., and Frank, M.: What Can We Learn From X-Ray Fluorescence Core Scanning Data? A Paleomonsoon Case Study, Geochem Geophys Geosyst, 21, e2019GC008414, https://doi.org/10.1029/2019GC008414, 2020.

R Core Team: R: A language and environment for statistical computing., Vienna, Austria, 2020.

Wickham, H.: ggplot2: Elegant graphics for data analysis, Springer, Cham, 140 pp., https://doi.org/10.1007/978-3-319-24277-4, 2016.